

NICST Internal Memo

Date: October 5, 2011
From: Jeff McIntire
To: Bruce Guenther, Jim Butler, and Jack Xiong
Subject: Uncertainty Estimate for the Thermal Band Radiometric Retrievals

References:

- [1] NICST_MEMO_11_001, 'Analysis of the Radiometric Calibration from VIIRS F1 RC-05 Part 1 Test (Nominal Plateau, Electronic Side B),' Jeff McIntire and Sanxiong Xiong, January 3, 2011.
- [2] NICST_MEMO_11_002, 'Analysis of the Radiometric Calibration from VIIRS F1 RC-05 Part 2 Test (Nominal Plateau),' Jeff McIntire and Sanxiong Xiong, January 31, 2011.
- [3] NICST_MEMO_11_003, 'Plateau and Electronics Side Comparison of Thermal Band Radiometric Calibration from VIIRS F1 RC-05 Testing,' Jeff McIntire, February 25, 2011.
- [4] An Introduction to Error Analysis, John R. Taylor, University Science Books, 1997.
- [5] 'Performance Verification Report – VIIRS FU1 Emissive Band Calibration (PVP Section 4.2.4),' Karen Galang, December 4, 2009, revision E.
- [6] PL3095-N06593, 'Absolute Radiometric Calibration Thermal Region: Uncertainty Estimates,' Jim Young, 1997.
- [7] NICST_MEMO_08_008, 'Response vs. Scan Angle for VIIRS FU1 TEB (FP-10, part 2),' Sanxiong Xiong, Chunhui Pan, and Nianzeng Che, March 11, 2008.
- [8] "VIIRS F1 BCS/OBC Temperature Offset Study Using RC-5 Part 1 and Part 2 Data, Updated," David Moyer and Frank De Luccia, April 1, 2011.
- [9] 'NPP Visible/infrared Imager Radiometer Suite (VIIRS) Radiance Uncertainty, Emissive Bands – Tested Performance', E. Johnson, K. Galang, C. Ranshaw, and Brendan Robinson, *Proc of SPIE* 7808, 78081F (2010).

1. Introduction

Thermal band radiometry was tested during RC-05 TV testing, the results of which were presented in [1-3]. This work will focus on propagating the uncertainty inherent in the measurement to the product level (radiance retrieval). The uncertainty is propagated using the standard formulation [4], as is described in the following section. Results of the error propagation are investigated under all instrument conditions (thermal vacuum instrument temperature plateaus and electronics sides), as well as using both the internal (OBC BB) and external (BCS) sources. The estimates contained in this work represent the uncertainties at the time of sensor level TV testing.

2. Error Propagation

For the purposes of this work, we follow the standard propagation of error as described by [4],

$$u^2(L_{ret}) = \sum_{i=1}^N \left(\frac{\partial L_{ret}}{\partial x_i} \right)^2 u^2(x_i) + 2 \sum_{i=1}^{N-1} \sum_{j=i+1}^N \left(\frac{\partial L_{ret}}{\partial x_i} \right) \left(\frac{\partial L_{ret}}{\partial x_j} \right) u(x_i, x_j). \quad (1)$$

Here $u(x_i)$ is the uncertainty of the underlying variable x_i that goes into the calculation of the radiance retrieval and $u(x_i, x_j)$ is the covariance between x_i and x_j . The EV retrieved radiance was defined in [1] and is a function of

$$L_{ret}^{EV} = f(c_0, c_1, c_2, L_{OBC}, L_{HAM}, L_{RTA}, L_{CAV}, L_{SH}, F_{SH}, F_{CAV}, F_{RTA}, RVS_{OBC}, RVS_{EV}, RVS_{SV}, \varepsilon_{OBC}, \rho_{RTA}, dn_{EV}, dn_{OBC}). \quad (2)$$

However, propagating the uncertainty at the retrieved radiance level includes some double counting, as the errors in the source path difference radiance are propagated into the fitting coefficient uncertainties as well as contribute at the retrieved radiance level. As a result, the uncertainties in the source path difference radiance were propagated into the coefficients errors using the random measurement error, and not included at the product level error propagation. This method will be described in the next section in greater detail.

The individual partial derivatives for each variable are listed in Appendix A for the OBC path difference radiance, Appendix B for the retrieved radiance using the BCS source, and Appendix C for the retrieved radiance using the OBC source. Note that the partial derivatives for the retrieved radiances do not include contributions that are included in the dependent variable of the least squares fitting.

In general, the covariance terms were not directly calculated (the exception is the covariance terms between the radiometric coefficients); a direct calculation of these terms is beyond the scope of this work.

3. Individual Error Sources

3.1 Radiances

The radiance uncertainty for each of the radiances that factor into the present calculation (L_{OBC} , L_{HAM} , L_{RTA} , L_{SH} , and L_{CAV}) is the RSS of the uncertainty contributors. Each of these radiances was converted from a temperature reading provided by one or more thermistors once per scan using the Planck equation, integrated over the spectral response of the instrument. In the cases where more than one thermistor was used, the average was employed in the Planck equation. The error is composed of two components: temperature and spectral uncertainty. The temperature uncertainties used in this analysis are listed in Table 1 [5]. The radiance uncertainty associated with each temperature error was determined by taking the absolute value of the difference between the Planck radiance with and without the temperature uncertainty, or

$$u(L) = \max(|L(T, \lambda) - L(T \pm \Delta T, \lambda)|). \quad (3)$$

The spectral errors used here are listed in Table 2 [6]. The radiance uncertainties due to spectral errors were determined in the same manner as the temperature uncertainties, $u(L) = \max(|L(T, \lambda) - L(T, \lambda \pm \Delta\lambda)|)$. (4)

3.2 Response Versus Scan (RVS)

The uncertainties for the RVS factors were determined in [7]. The RVS was normalized relative to the OBC HAM angle. The RVS uncertainty derived from FP-10 was a combination of fitting error and measurement error [7]; the band averaged values used in this work are given in Table 3. No uncertainty due to emission versus scan was included in the present work.

3.3 OBC Reflectance Shape Factors, Reflectance of the RTA, and Emissivity of the OBC

The uncertainties for the OBC reflectance shape factors are all taken to be 0.01 (the precision error of the calculation). The uncertainty for the reflectance of the RTA is 0.5% at 270 K [5]. This uncertainty was used for all source temperature levels. The OBC emissivity was measured at 3.39 μm ; the error in the emissivity measurement was determined to be 0.07% [5]. This uncertainty was used for all thermal bands.

3.4 EV and OBC Response

The uncertainty in the response was the RSS of the precision and accuracy errors for the background subtracted digital response. The precision error was the standard deviation over all analyzed samples and scans. The accuracy error was zero for the purposes of this work. Any bias common to all sectors would be removed in the background subtraction. The known biases between sectors have either been compensated for in the processing or are not applicable to the current analysis [5]:

- The EV response was reported in a truncated 12 bit format, whereas the calibration sectors were reported in 14 bits; this creates a bias of about 0.375 dn in the SV relative to the EV. To compensate in the analysis, all calibration view data was truncated to 12 bits at the beginning of the processing. The bias is then common to both sectors and is eliminated in the background subtraction.
- There is an additional bias in the EV data due to aggregation. In a three pixel aggregation zone, each pixel is truncated to 12 bits. Then the three pixels are averaged, and the average is truncated to 12 bits. A similar process was used for the two pixel aggregation zone. Because the testing was conducted in diagnostic mode, this bias does not effect the current calculation.
- For M13, there is a bias between fixed and auto gain configurations. Currently, the cause has not been determined [5]. The testing was conducted in fixed high gain, and as a result, this bias is not applicable to the present work.
- There is also a bias in the EV data for M16 TDI. Each M16A and M16B detector response is first truncated to 12 bits. Then the average of the two detector responses is taken, and that average is again truncated to 12 bits. Since this testing

was conducted in diagnostic mode, both M16A and M16B are reported instead of M16 TDI; consequently, this bias does not effect the current calculation.

3.6 Radiometric Coefficients

The vertical least-squares fitting algorithm used in this memo determined the vertical deviations of the set of data points from the fit, or

$$R^2 = \sum [\Delta L_i - c_0 - c_1 dn_i - c_2 dn_i^2]^2. \quad (5)$$

The minimum of the vertical deviations was computed by setting the partial derivatives with respect to coefficients equal to zero, or

$$\frac{\partial R^2}{\partial c_i} = 0. \quad (6)$$

This led to the following matrix equation:

$$\begin{bmatrix} c_0 \\ c_1 \\ c_2 \end{bmatrix} = \begin{bmatrix} N & \sum dn & \sum dn^2 \\ \sum dn & \sum dn^2 & \sum dn^3 \\ \sum dn^2 & \sum dn^3 & \sum dn^4 \end{bmatrix}^{-1} \begin{bmatrix} \sum \Delta L \\ \sum dn \Delta L \\ \sum dn^2 \Delta L \end{bmatrix}, \quad (7)$$

where N is the number of points used in the fit and we define

$$A = \begin{bmatrix} N & \sum dn & \sum dn^2 \\ \sum dn & \sum dn^2 & \sum dn^3 \\ \sum dn^2 & \sum dn^3 & \sum dn^4 \end{bmatrix}^{-1}. \quad (8)$$

The solution to this matrix equation determined the radiometric coefficients used in previous work [1-3]. This algorithm also produced 1-sigma uncertainties and covariance terms. The variance of the fitting points with respect to the fit was determined by

$$\sigma_{fit}^2 = \frac{1}{N-3} \sum_{i=1}^N (\Delta L_i - c_0 - c_1 dn_i - c_2 dn_i^2)^2, \quad (9)$$

which is a indicator of the error in the measurements. The coefficient uncertainties and covariance terms are defined by the following:

$$u(c_i) = \sigma_{fit}^2 \sqrt{A(i,i)}, \quad (10)$$

$$u(c_i, c_j) = \sigma_{fit}^2 A(i,j). \quad (11)$$

This approach assumes that the uncertainties in ΔL are roughly constant over the data points used (and uncertainties in dn are negligible). However, this algorithm only included some effects from precision error (random statistical variations), but excluded any bias uncertainties (accuracy error). Furthermore, it should be noted that the uncertainties are valid only insomuch as the model itself is valid. The quality of the radiometric fitting for the thermal bands has been discussed in previous work [1-3]; in addition, an initial investigation into quality of the model is contained in a later section. For the purposes of this memo, the radiometric model is considered sufficiently valid to proceed with the uncertainty analysis.

The above procedure was followed at each instrument condition (temperature plateaus and electronics sides) as well as for both internal and external sources. The radiometric fitting was conducted on a collect basis using the BCS source, whereas the fitting was

performed on a scan by scan basis when using the OBC source (it was not possible to conduct scan by scan fitting for the BCS due to a lack of data). In the present calculation, the uncertainty using the OBC was propagated over all scans by taking the mean uncertainty divided by the square root of the number of scans.

3.7 Model Validity

As stated above, the radiometric fitting results are valid only inasmuch as the model itself is valid. There are two sources of model uncertainty which are considered here: biases and functional form. An investigation of the model biases was performed by Moyer [8] in which a parametric model was used to vary the parameters in the radiometric model in order to minimize the ARD. It was determined that a bias existed between the BCS and OBC sources of roughly 50 mK (this is below the stated uncertainties for these sources). Results were consistent between RC-05 part 1 (BCS varying with the OBC fixed) and part 2 (OBC varying with the BCS fixed).

In addition, the functional form of the model was investigated by varying the order of the polynomial used in the fitting. Linear, quadratic, and cubic polynomials were employed. The full error analysis was conducted for each, and the results were compared to determine any relative improvement in fitting with increasing polynomial order.

4. Results

Figures 1 and 2 plot the individual uncertainty contributors for path difference radiance (ΔL_{OBC}) for each band (detector 9) using data from RC-05 part 1 at Nominal plateau, electronics side B. For the MWIR, the OBC radiance error was the leading term at approximately 0.3 % for all scene temperatures; all other contributors for all other bands were below 0.1 %.

Figures 3 – 10 graph the individual uncertainty contributors for the EV retrieved radiance using data from RC-05 part 1 at Nominal plateau, electronics side B (detector 9). The contribution from ΔL_{OBC} was about 3 % for the MWIR, 2 % for M14, and 1 % for the remaining LWIR. This factor was roughly constant over scene temperature (decreasing slightly at very low temperatures). The ΔL_{OBC} uncertainty was dominant above about 250 K for the MWIR and at all scene temperatures for the LWIR. For the MWIR, the c_0 error was the largest contributor below 250 K; the remaining terms were in general negligible (note that there was a small negative covariance term between c_0 and c_2).

The total uncertainties for the EV retrieved radiance are shown in Figures 11 and 12 using data from RC-05 part 1 at Nominal plateau, electronics side B (detector 9). In addition, the TV results (the RSS of the maximum ARD [1] and a 50 mK bias in the BCS temperature) and Raytheon BOL estimates [9] are also plotted. The calculated uncertainties show reasonable agreement with the measured results. For the MWIR, the TV results increased rapidly below a higher scene temperature (about 270 K) than the model (closer to 250 K); in addition, the structure in the TV results for I4 or M13 above 270 K was not observed in either model (this structure was mostly due to fitting residual

contributions). Raytheon's modeled results [9] are in general larger than the modeled results shown here.

The plots in Figures 13 and 14 show the total uncertainties across instrument temperatures and electronic sides for all bands (detector 9). The uncertainty estimates were very consistent over instrument conditions for all bands, except at the lowest scene temperatures, where some slight variation was observed. It should be noted that the temperature and spectral biases as well as RVS uncertainties (the terms that dominate the error propagation) used in this work were independent of instrument condition.

Figures 15 (I4) and 16 (M14) show the investigation of polynomial order on the modeled results. Linear, quadratic, and cubic fits were performed, and the error propagation conducted separately for each (graphed in the upper, middle, and lower plots respectively). The modeled results (black) are shown alongside the maximum ARD (red) for each case. In general, only marginal improvement in the fitting was derived by increasing the polynomial order from 2 to 3; in contrast, the quadratic model was a significant improvement over the linear (especially for M14). The I4 and M14 results are representative of the MWIR and LWIR behaviors.

The individual uncertainty contributors to the OBC retrieved radiance for each band using RC-05 part 2 data from Nominal plateau, electronics side B are shown in Figures 17 – 24. The coefficient errors were much larger than in part 1 data, especially in the LWIR bands. The uncertainties in the three coefficients and the covariance term between $c_0 - c_2$ were all positive and non-negligible; the covariance terms between $c_0 - c_1$ and $c_1 - c_2$ were negative and also non-negligible.

However, when the individual uncertainties were combined via the propagation equations described above, the total uncertainties were small (on the order of 0.1 % or less). Here an additional bias term was introduced for the OBC of 0.04 K [using Eqs. (3) and (4)] due to the fact that the OBC uncertainty did not enter into the propagation (only statistical uncertainties are contained in the coefficient fitting errors). This additional term raised the overall uncertainty for the MWIR to around 0.4 – 0.6 %, decreasing slightly with increasing OBC temperature; the LWIR overall uncertainty was approximately 0.1 % at all scene temperatures. The modeled results were in good agreement with the measured values for all bands. Figures 25 and 26 graph the total uncertainties for each band along with the maximum OBC ARD for Nominal plateau, electronic side B data (detector 9).

Figures 27 and 28 show the variation of the total uncertainty with temperature plateau; as the dominant term was the OBC temperature uncertainty (which was not varied with instrument temperature), the different instrument conditions were largely in agreement.

5. Summary

Uncertainty estimates for the thermal band radiometry retrievals were determined by propagating the error estimates from the individual uncertainty sources. This uncertainty

model was applied to cases using both the internal (OBC BB) and external (BCS) sources as well as too various instrument conditions. The following is a list of findings:

- In general, the modeled uncertainty estimates were in good agreement with the measured radiance retrieval errors.
- MWIR EV retrieved radiance uncertainties are between 0.3 – 0.4 % at high scene temperatures and increase rapidly below 250 – 270 K. LWIR EV retrieved radiance uncertainties are between 0.1 – 0.2 % over all scene temperatures
- Dominant terms in MWIR EV uncertainties are OBC radiance error at high scene temperatures and c_0 coefficient uncertainties at lower scene temperatures (below about 260 K). The dominant term in LWIR EV uncertainties was the OBC radiance error at all scene temperatures.
- Improvement in model uncertainty form increasing polynomial order to cubic was small.
- Uncertainties derived using the OBC BB decreased from 0.6 to 0.4 % for the MWIR and were roughly constant around 0.1 % for the LWIR over the range of OBC temperatures. The dominant term is the OBC radiance uncertainty. Results are roughly consistent with those derived for the EV.
- Changes in instrument condition (temperature plateau or electronic side) have limited impact.

Appendix A

The following are the partial derivatives of the OBC path difference radiance with respect to the various contributors:

$$\begin{aligned} \frac{\partial \Delta L_{OBC}}{\partial rvs_{OBC}} &= \varepsilon_{OBC} L_{OBC} + (1 - \varepsilon_{OBC}) (F_{SH} L_{SH} + F_{CAV} L_{CAV} + F_{RTA} L_{RTA}) - \frac{1}{\rho_{RTA}} [L_{HAM} - (1 - \rho_{RTA}) L_{RTA}] \\ \frac{\partial \Delta L_{OBC}}{\partial rvs_{SV}} &= L_{SV} + \frac{1}{\rho_{RTA}} [L_{HAM} - (1 - \rho_{RTA}) L_{RTA}] \\ \frac{\partial \Delta L_{OBC}}{\partial L_{OBC}} &= \varepsilon_{OBC} \\ \frac{\partial \Delta L_{OBC}}{\partial L_{SV}} &= -rvs_{SV} \\ \frac{\partial \Delta L_{OBC}}{\partial L_{HAM}} &= \frac{(rvs_{SV} - 1)}{\rho_{RTA}} \\ \frac{\partial \Delta L_{OBC}}{\partial L_{RTA}} &= (1 - \varepsilon_{OBC}) F_{RTA} - \frac{(rvs_{SV} - 1)}{\rho_{RTA}} (1 - \rho_{RTA}) \\ \frac{\partial \Delta L_{OBC}}{\partial \varepsilon_{OBC}} &= L_{OBC} - (F_{SH} L_{SH} + F_{CAV} L_{CAV} + F_{RTA} L_{RTA}) \\ \frac{\partial \Delta L_{OBC}}{\partial \rho_{RTA}} &= -\frac{(rvs_{SV} - 1)}{\rho_{RTA}^2} (L_{HAM} - L_{RTA}) \end{aligned}$$

$$\frac{\partial \Delta L_{OBC}}{\partial F_{SH}} = (1 - \varepsilon_{OBC}) L_{SH}$$

$$\frac{\partial \Delta L_{OBC}}{\partial F_{CAV}} = (1 - \varepsilon_{OBC}) L_{CAV}$$

$$\frac{\partial \Delta L_{OBC}}{\partial F_{RTA}} = (1 - \varepsilon_{OBC}) L_{RTA}$$

$$\frac{\partial \Delta L_{OBC}}{\partial L_{SH}} = (1 - \varepsilon_{OBC}) F_{SH}$$

$$\frac{\partial \Delta L_{OBC}}{\partial L_{CAV}} = (1 - \varepsilon_{OBC}) F_{CAV}$$

Appendix B

The following are the partial derivatives of the retrieved EV radiance with respect to the various contributors:

$$\frac{\partial L_{EV}^{ret}}{\partial \Delta L_{OBC}} = \frac{(c_0 + c_1 dn_{EV} + c_2 dn_{EV}^2)}{rvs_{EV} (c_0 + c_1 dn_{OBC} + c_2 dn_{OBC}^2)}$$

$$\frac{\partial L_{EV}^{ret}}{\partial c_0} = \frac{\Delta L_{OBC}}{rvs_{EV}} \frac{c_1 (dn_{OBC} - dn_{EV}) + c_2 (dn_{OBC}^2 - dn_{EV}^2)}{(c_0 + c_1 dn_{OBC} + c_2 dn_{OBC}^2)^2}$$

$$\frac{\partial L_{EV}^{ret}}{\partial c_1} = \frac{\Delta L_{OBC}}{rvs_{EV}} \frac{c_0 (dn_{EV} - dn_{OBC}) + c_2 (dn_{OBC}^2 dn_{EV} - dn_{EV}^2 dn_{OBC})}{(c_0 + c_1 dn_{OBC} + c_2 dn_{OBC}^2)^2}$$

$$\frac{\partial L_{EV}^{ret}}{\partial c_2} = \frac{\Delta L_{OBC}}{rvs_{EV}} \frac{c_0 (dn_{EV}^2 - dn_{OBC}^2) + c_1 (dn_{EV}^2 dn_{OBC} - dn_{OBC}^2 dn_{EV})}{(c_0 + c_1 dn_{OBC} + c_2 dn_{OBC}^2)^2}$$

$$\frac{\partial L_{EV}^{ret}}{\partial dn_{EV}} = \frac{\Delta L_{OBC}}{rvs_{EV}} \frac{c_1 + 2c_2 dn_{EV}}{(c_0 + c_1 dn_{OBC} + c_2 dn_{OBC}^2)}$$

$$\frac{\partial L_{EV}^{ret}}{\partial dn_{OBC}} = \frac{\Delta L_{OBC}}{rvs_{EV}} \frac{(c_1 + 2c_2 dn_{OBC})(c_0 + c_1 dn_{EV} + c_2 dn_{EV}^2)}{(c_0 + c_1 dn_{OBC} + c_2 dn_{OBC}^2)^2}$$

Appendix C

The following are the partial derivatives of the retrieved OBC radiance with respect to the various contributors:

$$\frac{\partial L_{OBC}^{ret}}{\partial c_0} = 1$$

$$\frac{\partial L_{OBC}^{ret}}{\partial c_1} = dn_{OBC}$$

$$\frac{\partial L_{OBC}^{ret}}{\partial c_2} = dn_{OBC}^2$$

$$\frac{\partial L_{OBC}^{ret}}{\partial dn_{OBC}} = (c_1 + 2c_2 dn_{OBC})$$

Acknowledgement

The sensor test data used in this document was provided by the Raytheon El Segundo testing team. Approaches for data acquisition and data reductions, as well as data extraction tools were also provided by the Raytheon El Segundo team. We would like to thank the Raytheon El Segundo team for their support. The data analysis tools were developed by the NICST team.

Table 1: Temperature biases [5].

Source	Temperature Bias (K)
OBC	0.04
HAM	1.0
RTA	9.0
SH	3.0
CAV	6.0

Table 2: Spectral biases [6].

Band	Spectral Bias (nm)
I4	1.2
I5	4.0
M12	1.2
M13	1.2
M14	4.0
M15	4.0
M16A	4.0
M16B	4.0

Table 3: RVS uncertainties [7].

Band	RVS uncertainty
I4	0.000811
I5	0.000986
M12	0.000818
M13	0.000798
M14	0.001003
M15	0.000875
M16A	0.000804
M16B	0.000759

Figure 1: Uncertainty contributors in ΔL_{OBC} (Nominal plateau, electronics side B).

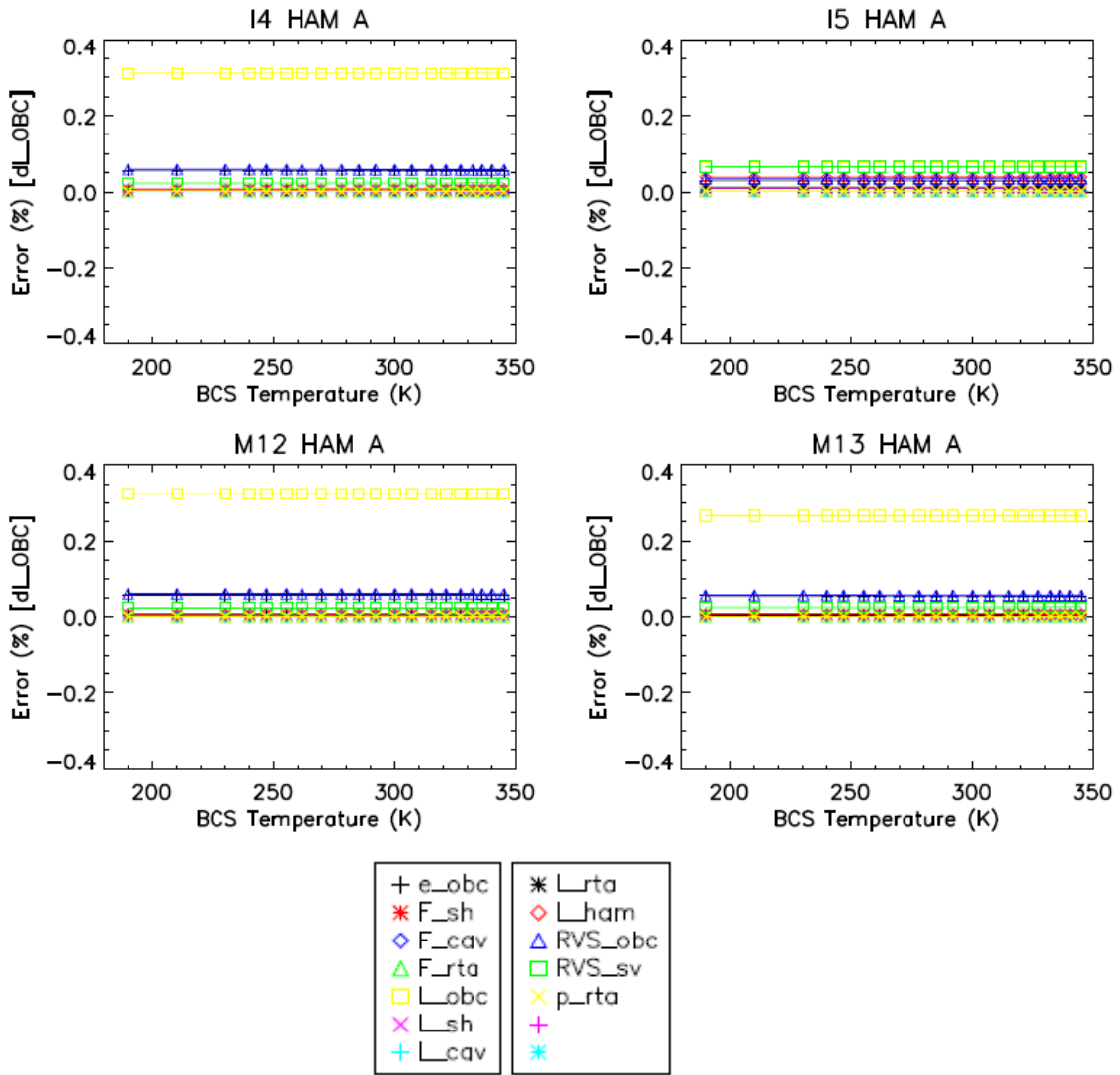


Figure 2: Uncertainty contributors in ΔL_{OBC} (Nominal plateau, electronics side B).

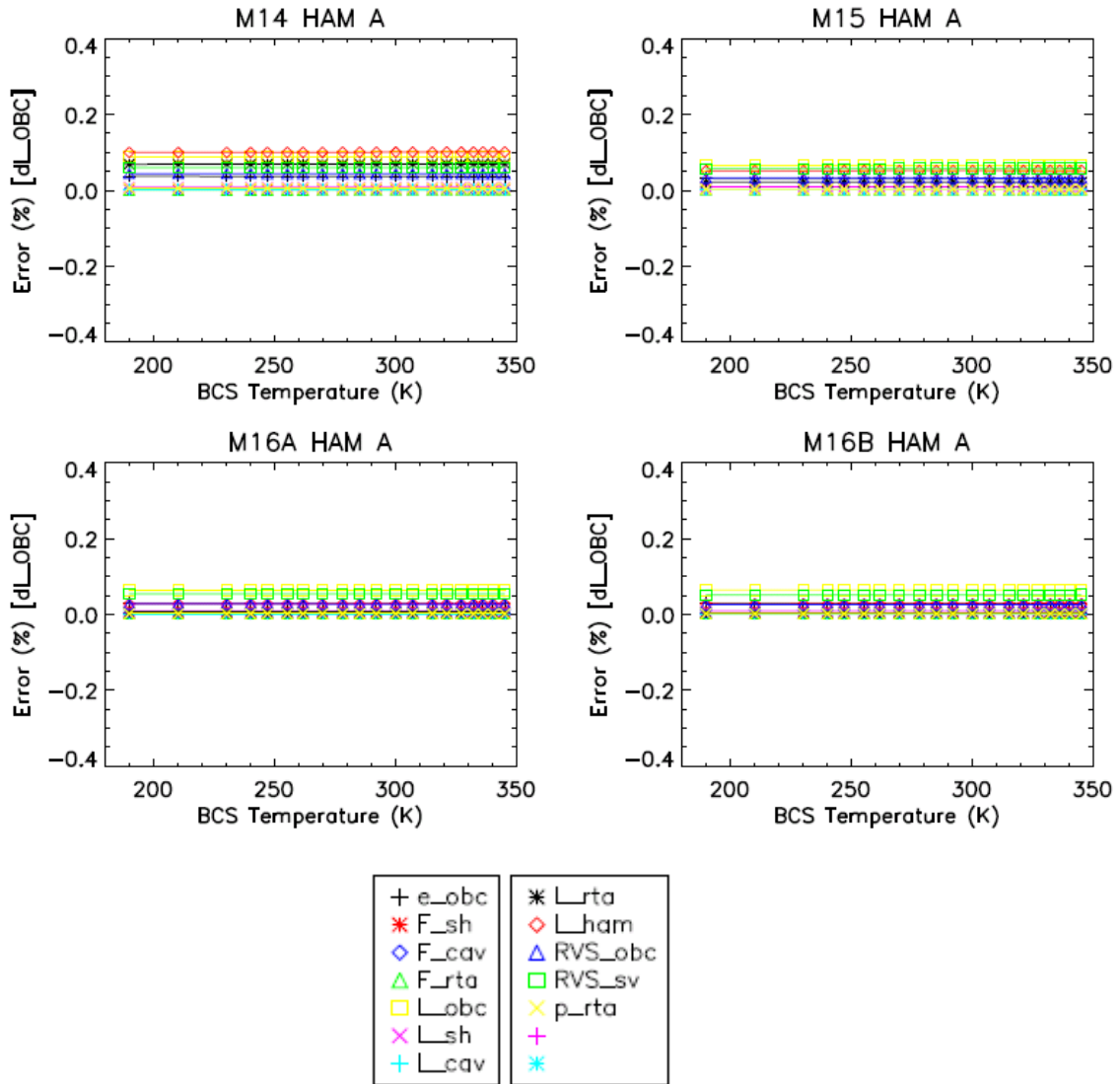


Figure 3: I4 individual uncertainty terms in EV L_{ret} (Nominal plateau, electronics side B).

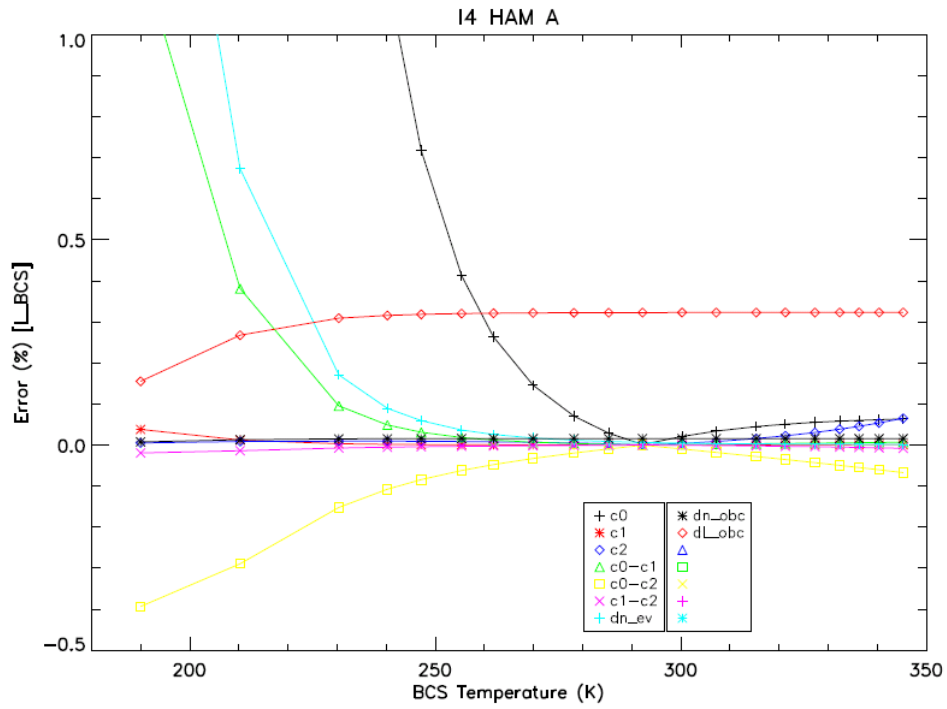


Figure 4: I5 individual uncertainty terms in EV L_{ret} (Nominal plateau, electronics side B).

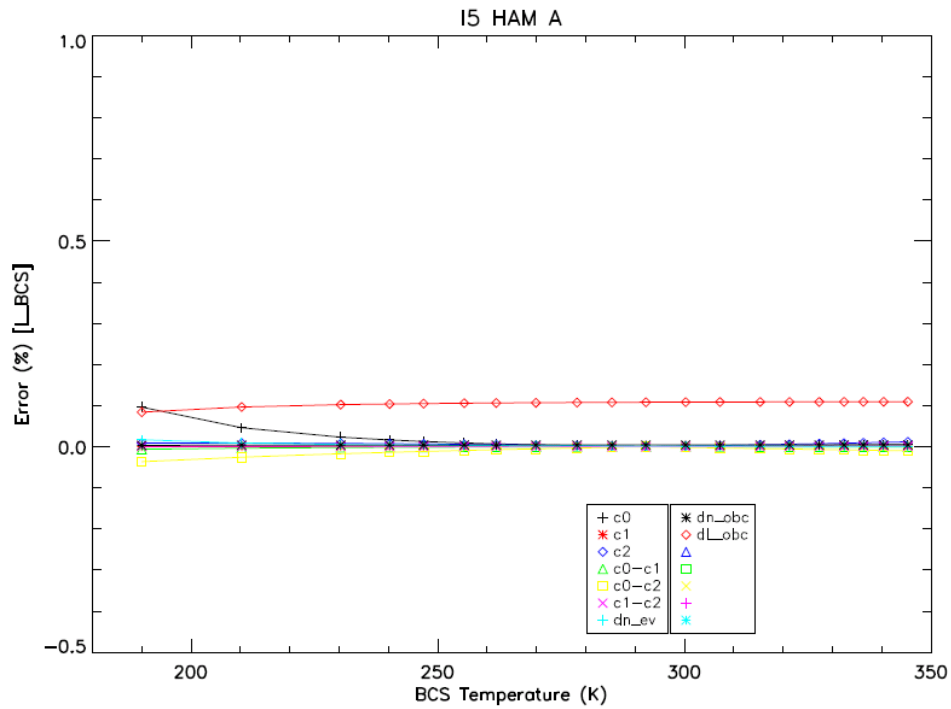


Figure 5: M12 individual uncertainty terms in EV L_{ret} (Nominal plateau, electronics side B).

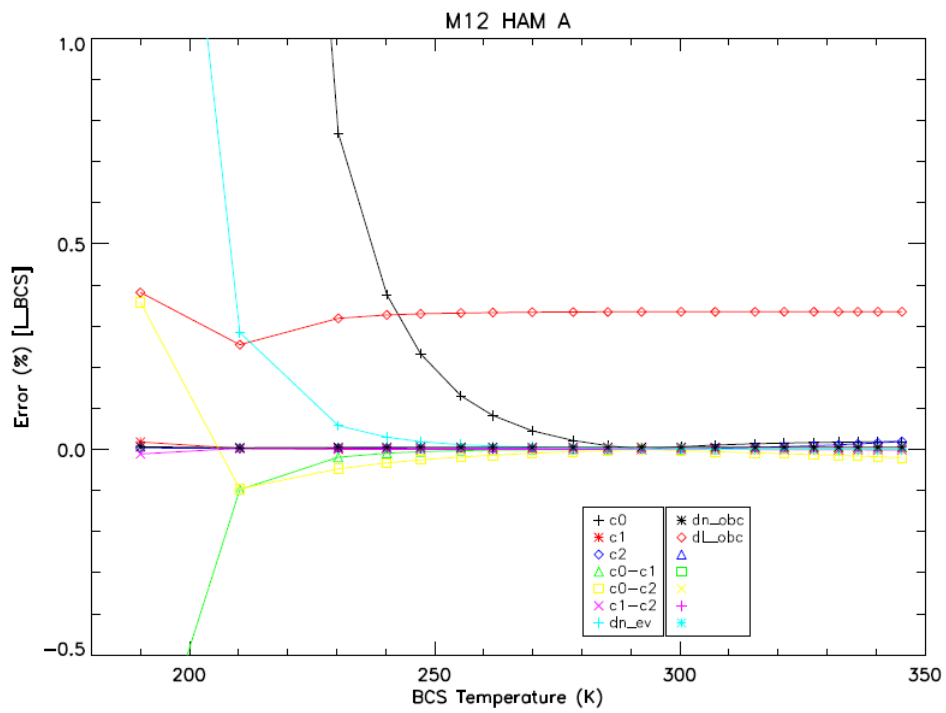


Figure 6: M13 individual uncertainty terms in EV L_{ret} (Nominal plateau, electronics side B).

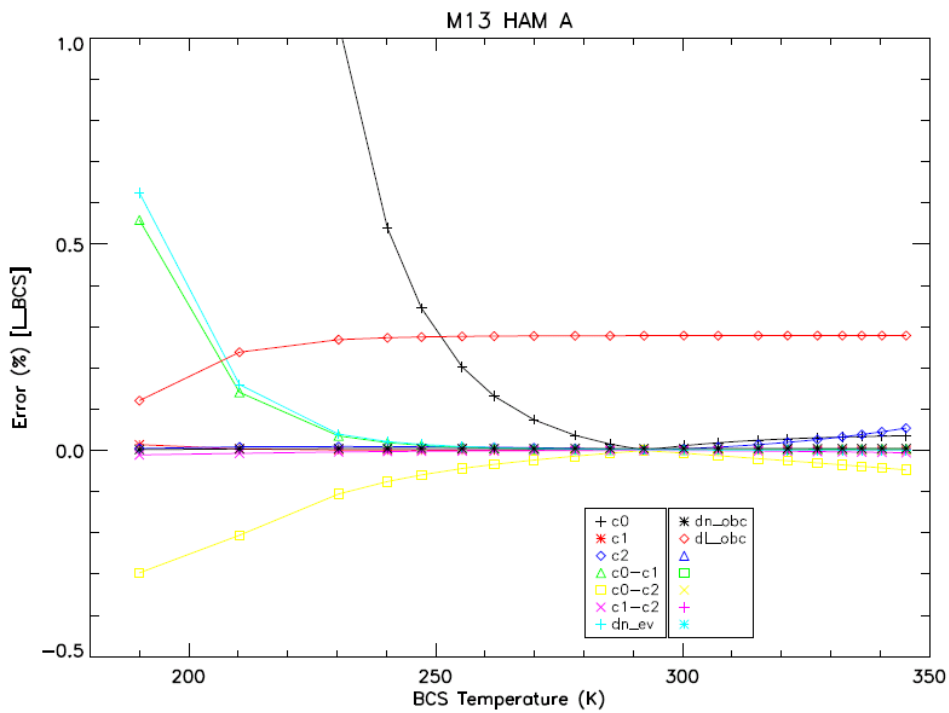


Figure 7: M14 individual uncertainty terms in EV L_{ret} (Nominal plateau, electronics side B).

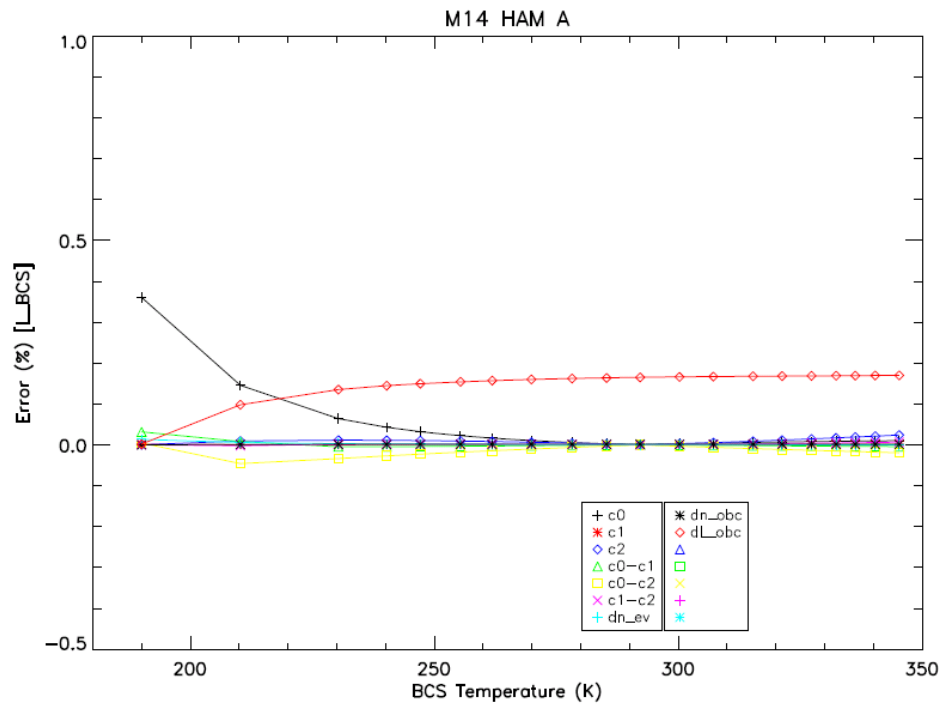


Figure 8: M15 individual uncertainty terms in EV L_{ret} (Nominal plateau, electronics side B).

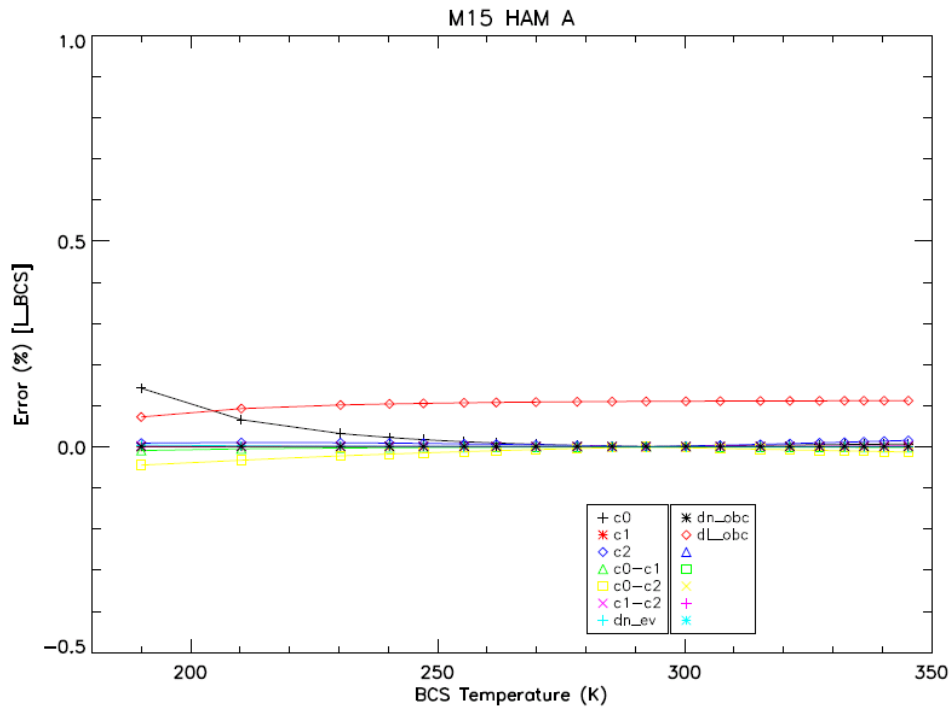


Figure 9: M16A individual uncertainty terms in EV L_{ret} (Nominal plateau, electronics side B).

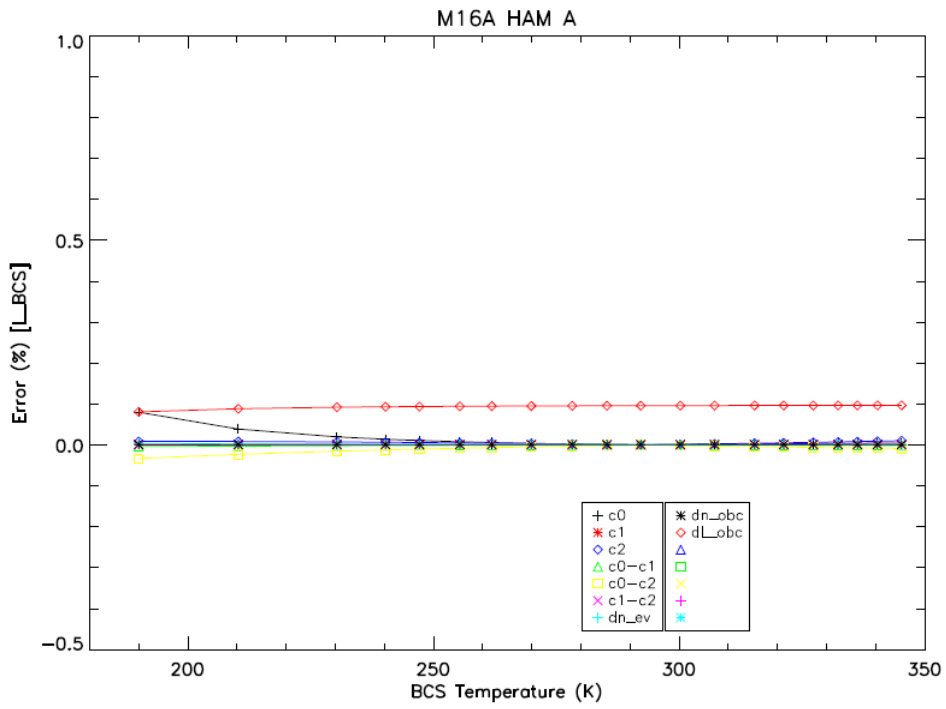


Figure 10: M16B individual uncertainty terms in EV L_{ret} (Nominal plateau, electronics side B).

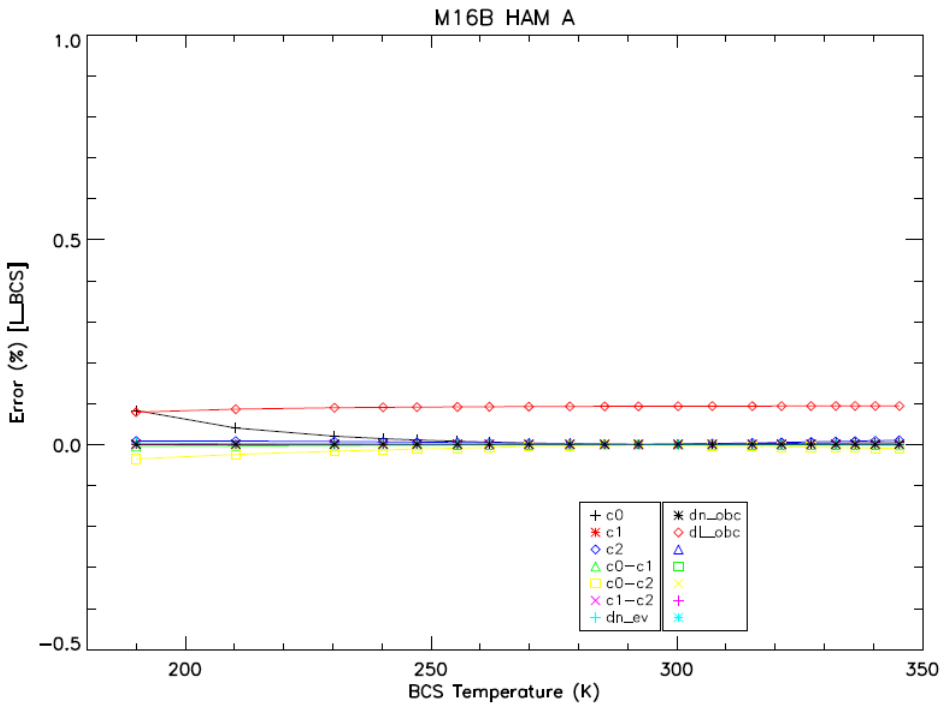


Figure 11: Total uncertainties in EV L_{ret} (Nominal plateau, electronics side B).

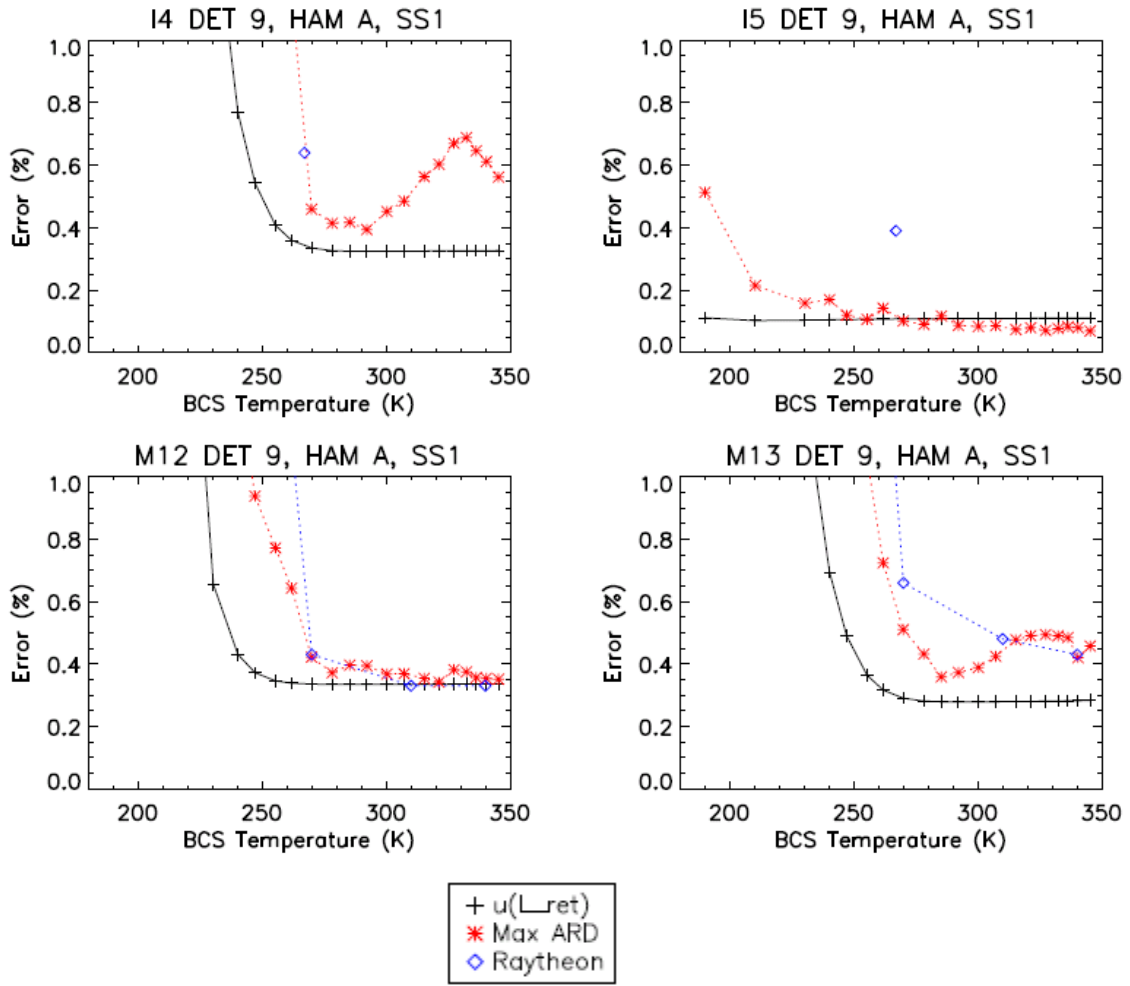


Figure 12: Total uncertainties in EV L_{ret} (Nominal plateau, electronics side B).

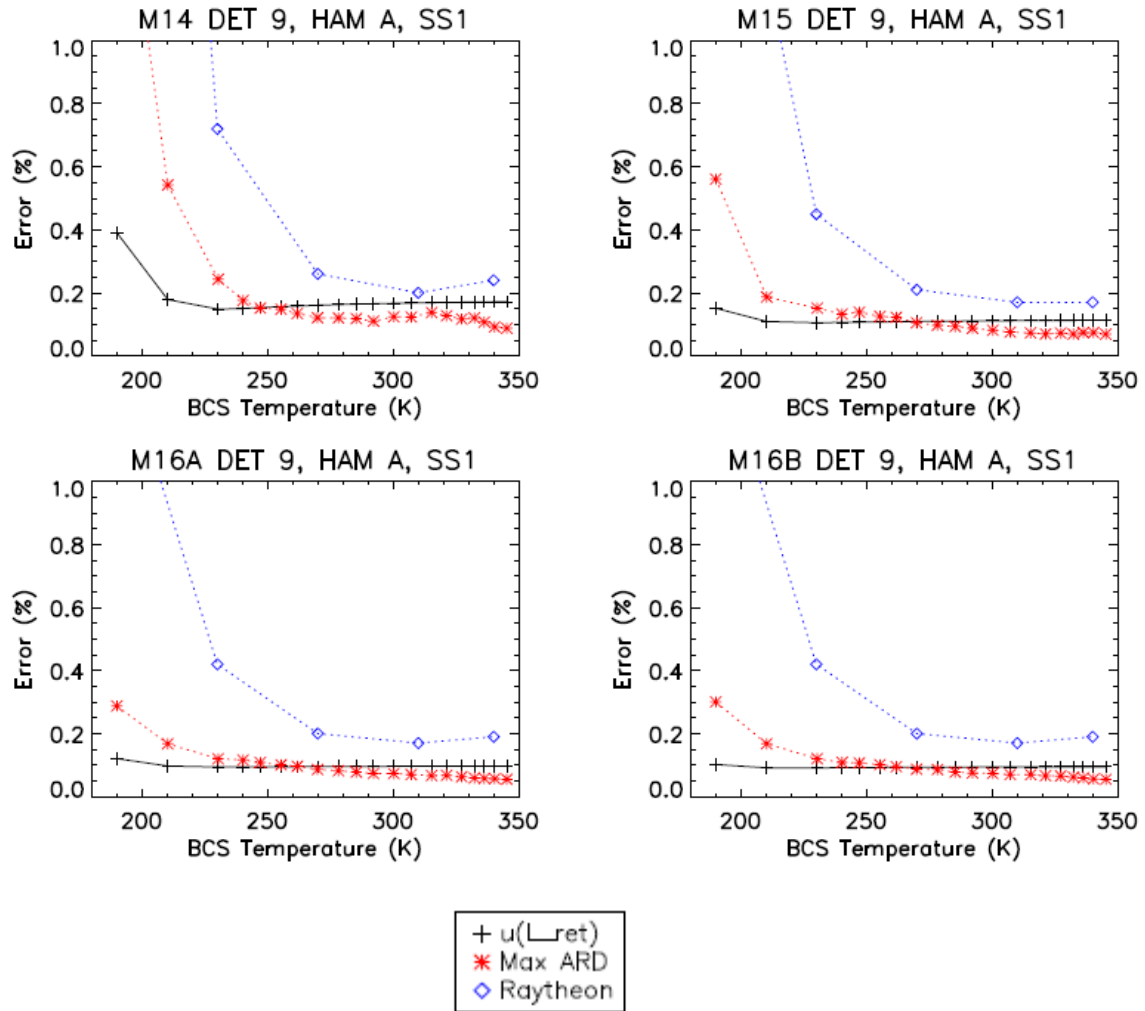


Figure 13: Total uncertainties in EV L_{ret} across instrument conditions.

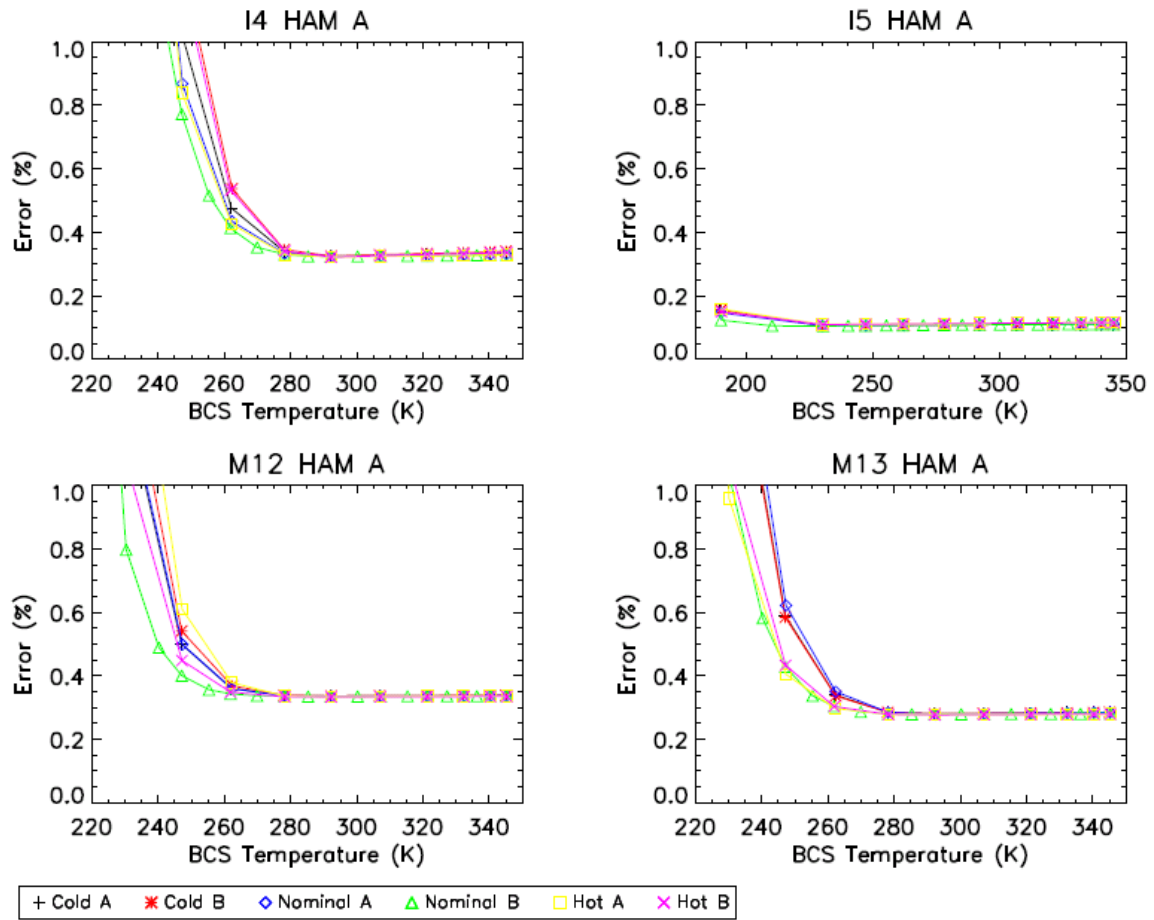


Figure 14: Total uncertainties in EV L_{ret} across instrument conditions.

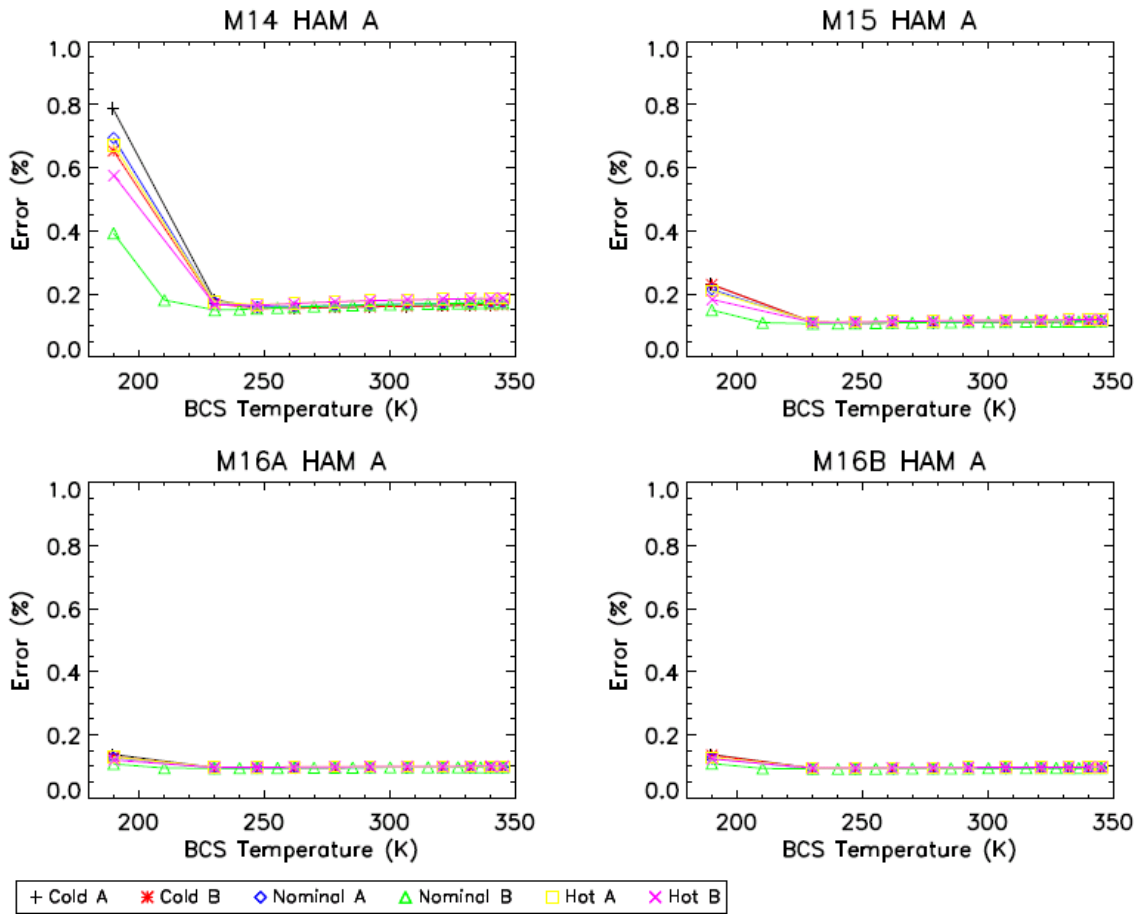


Figure 15: Model differences between linear, quadratic, and cubic polynomials (I4, Nominal plateau, electronics side B).

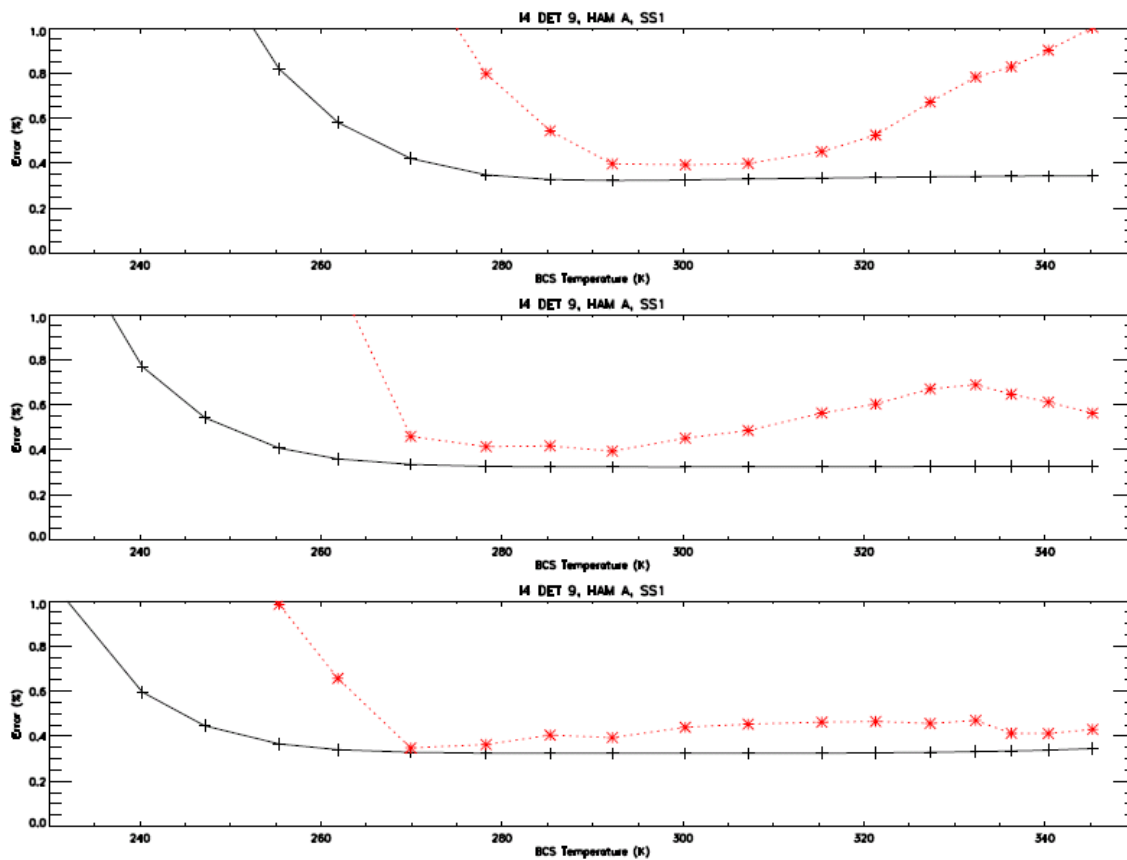


Figure 16: Model differences between linear, quadratic, and cubic polynomials (M14, Nominal plateau, electronics side B).

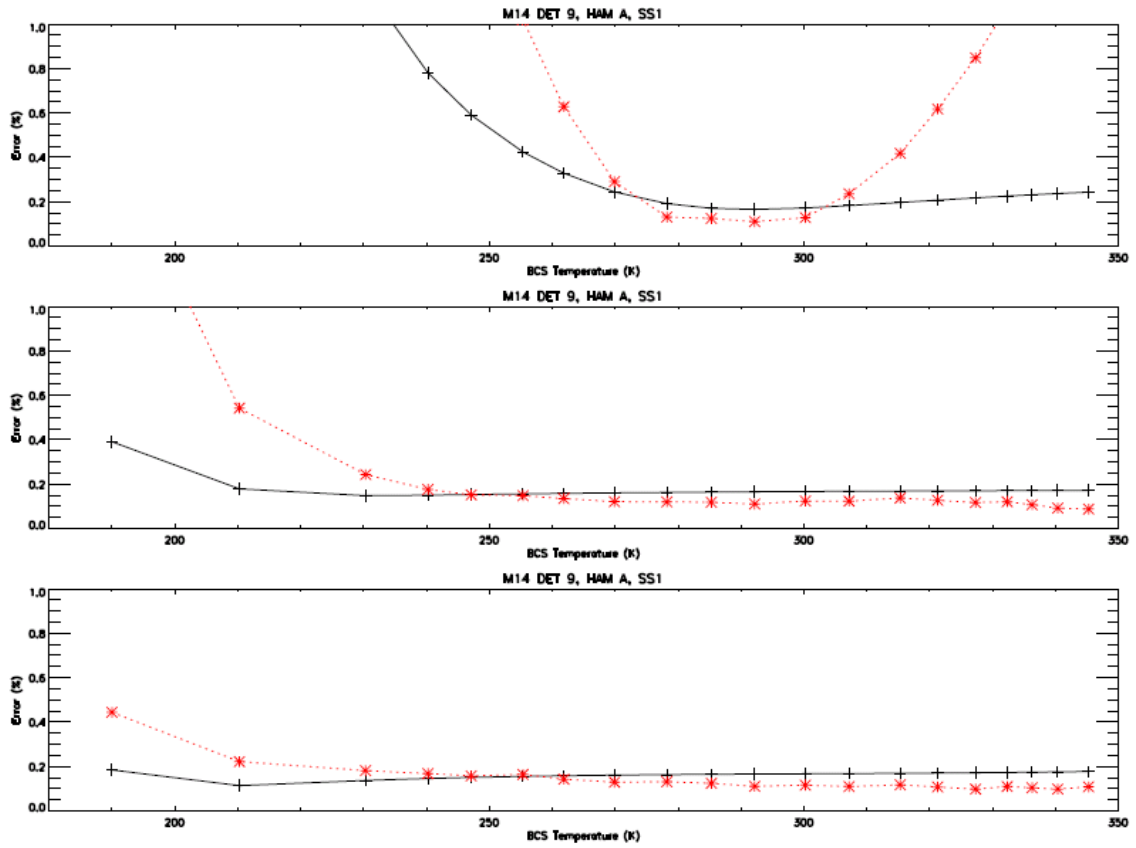


Figure 17: I4 individual uncertainty terms in OBC L_{ret} (Nominal plateau, electronics side B).

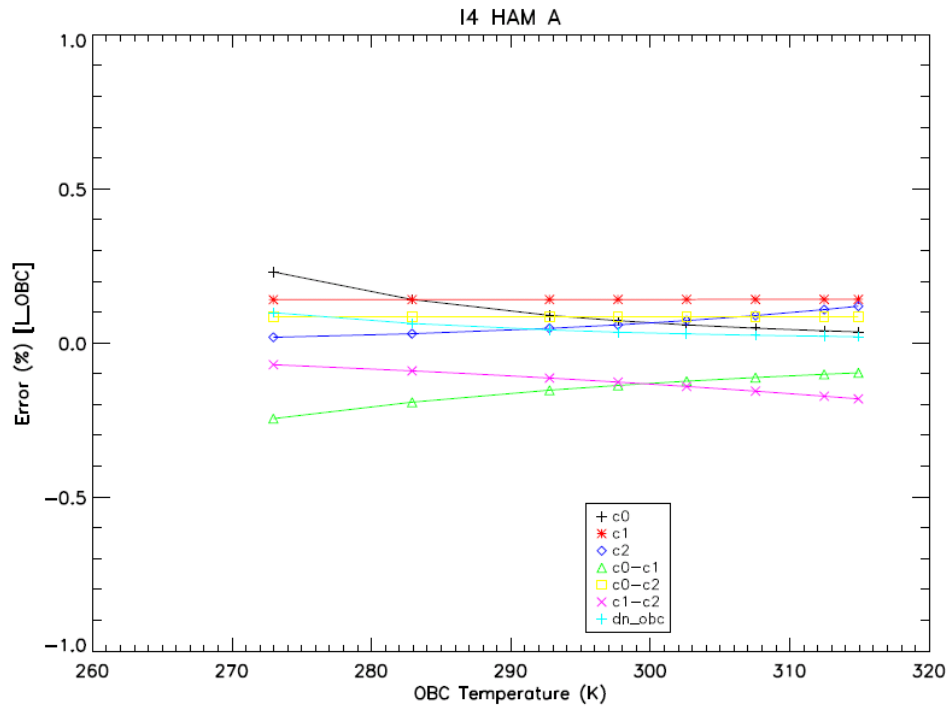


Figure 18: I5 individual uncertainty terms in OBC L_{ret} (Nominal plateau, electronics side B).

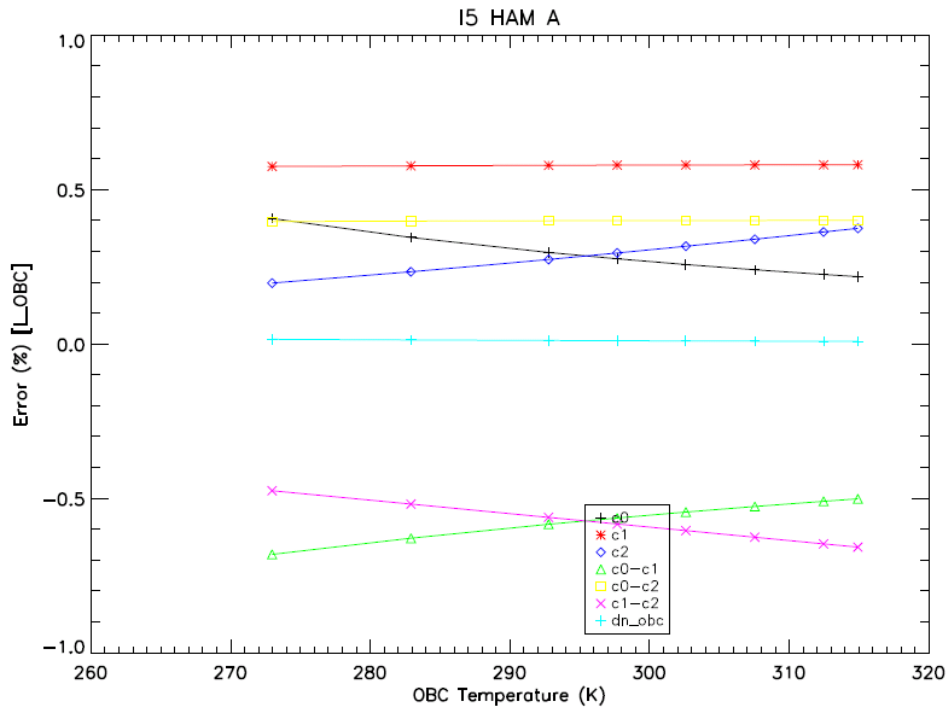


Figure 19: M12 individual uncertainty terms in OBC L_{ret} (Nominal plateau, electronics side B).

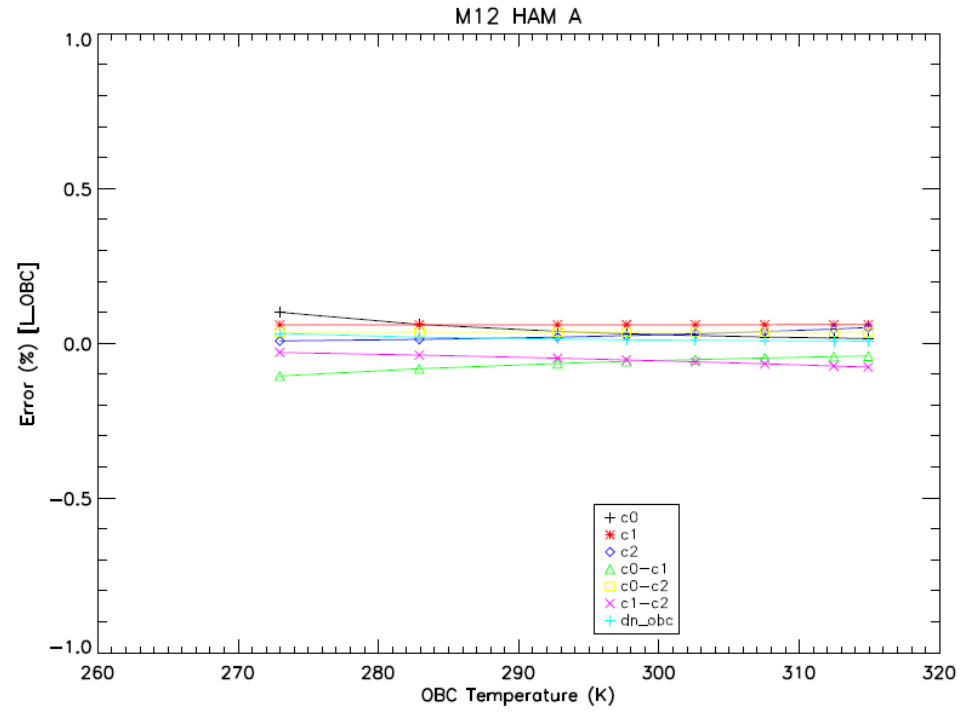


Figure 20: M13 individual uncertainty terms in OBC L_{ret} (Nominal plateau, electronics side B).

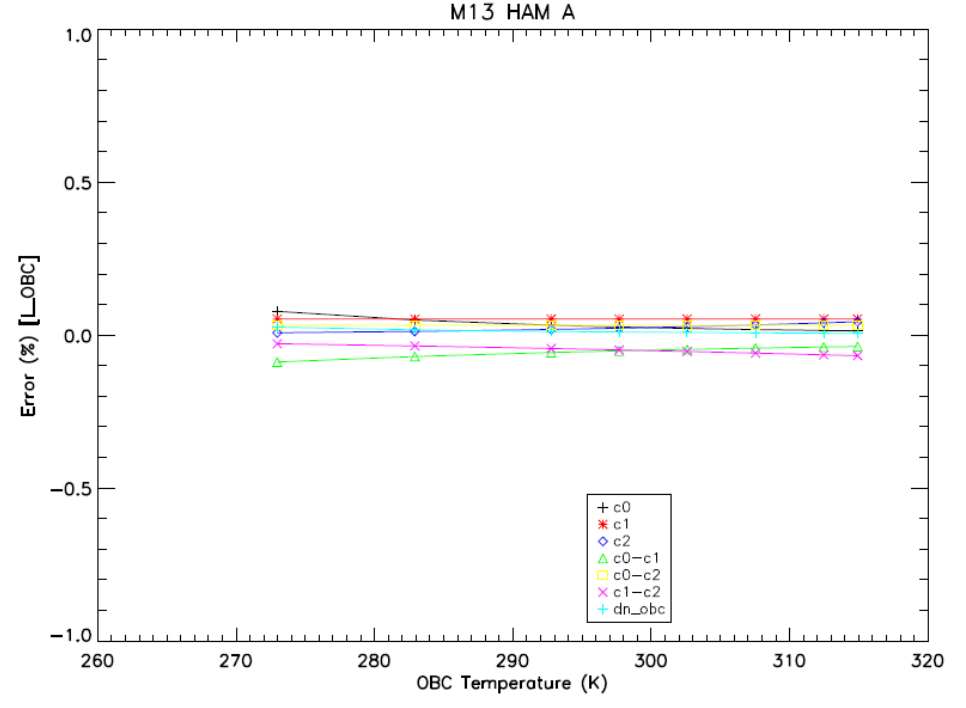


Figure 21: M14 individual uncertainty terms in OBC L_{ret} (Nominal plateau, electronics side B).

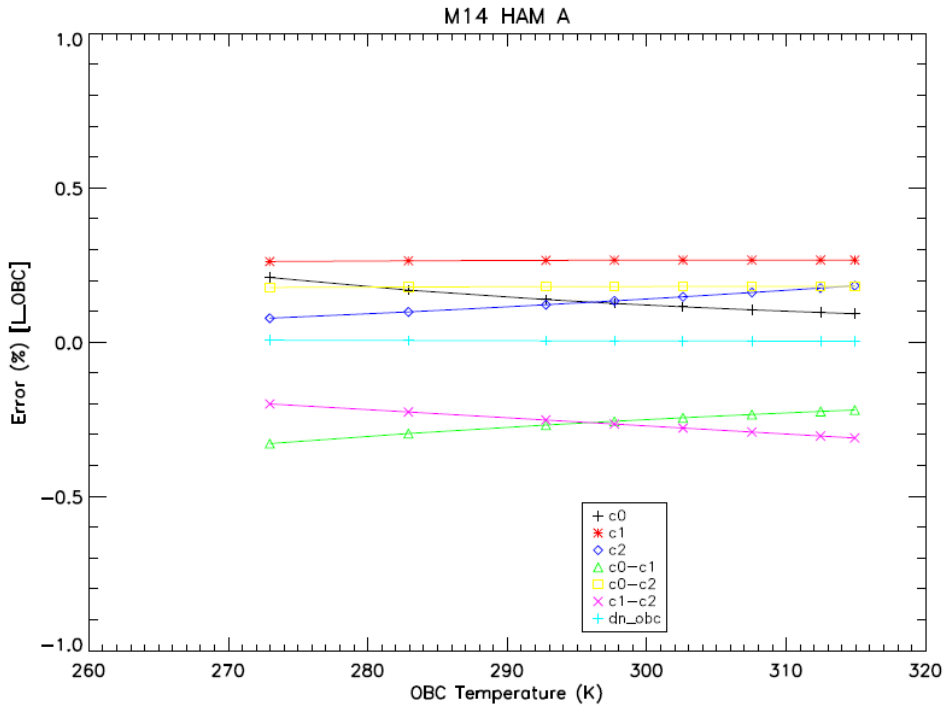


Figure 22: M15 individual uncertainty terms in OBC L_{ret} (Nominal plateau, electronics side B).

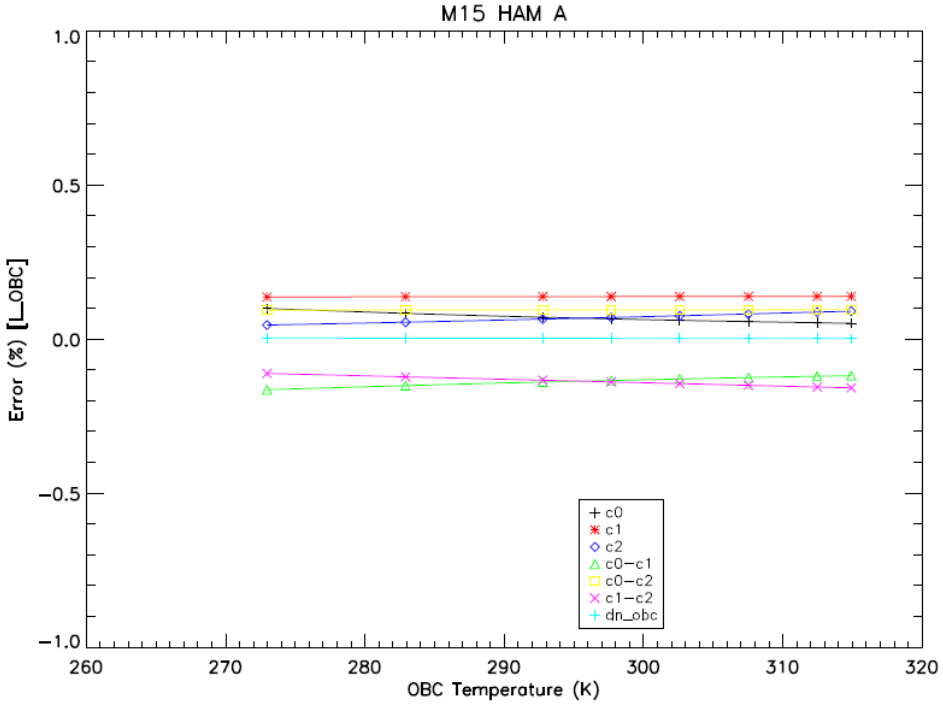


Figure 23: M16A individual uncertainty terms in OBC L_{ret} (Nominal plateau, electronics side B).

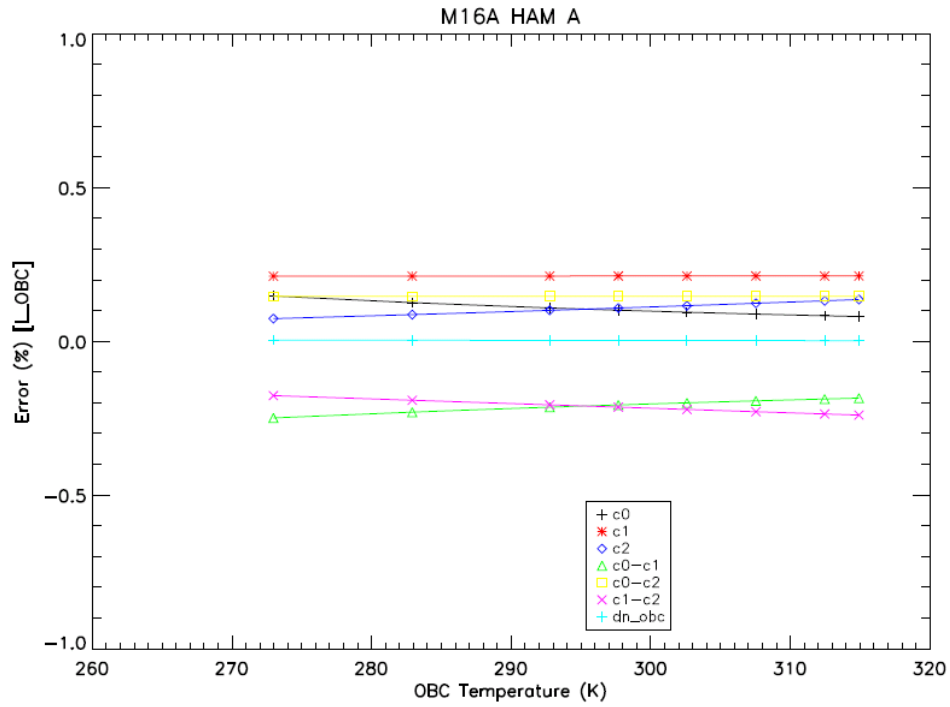


Figure 24: M16B individual uncertainty terms in OBC L_{ret} (Nominal plateau, electronics side B).

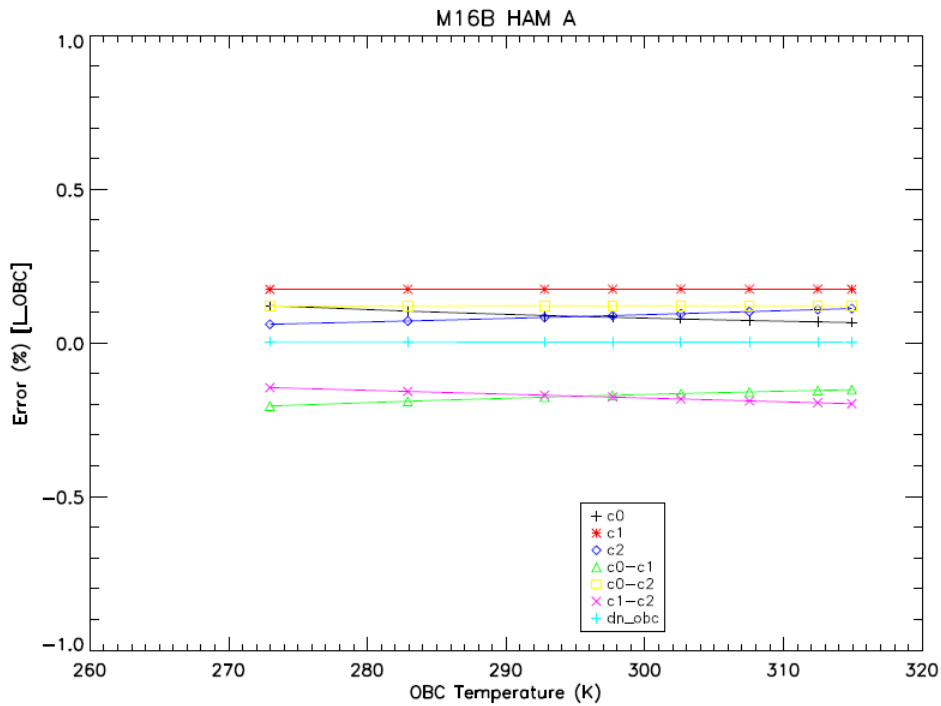


Figure 25: Total uncertainties OBC L_{ret} (Nominal plateau, electronics side B).

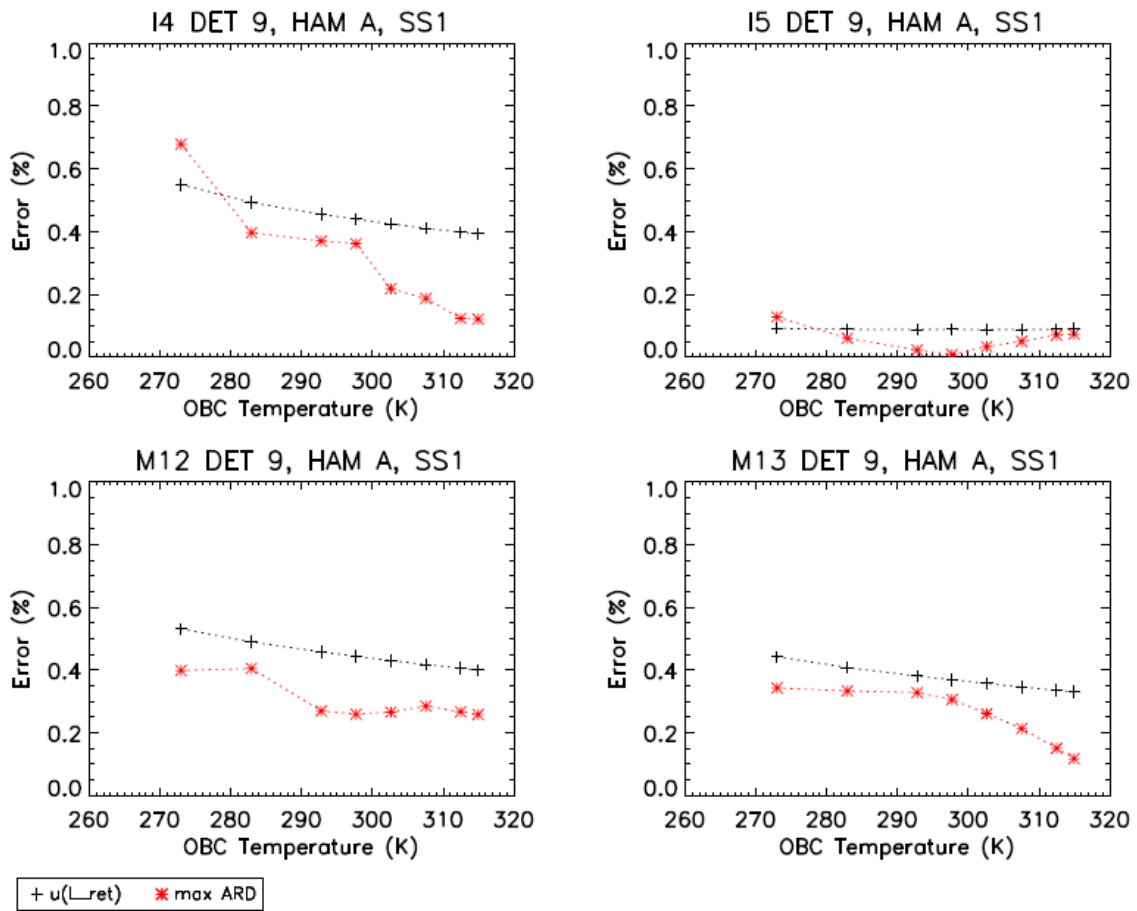


Figure 26: Total uncertainties OBC L_{ret} (Nominal plateau, electronics side B).

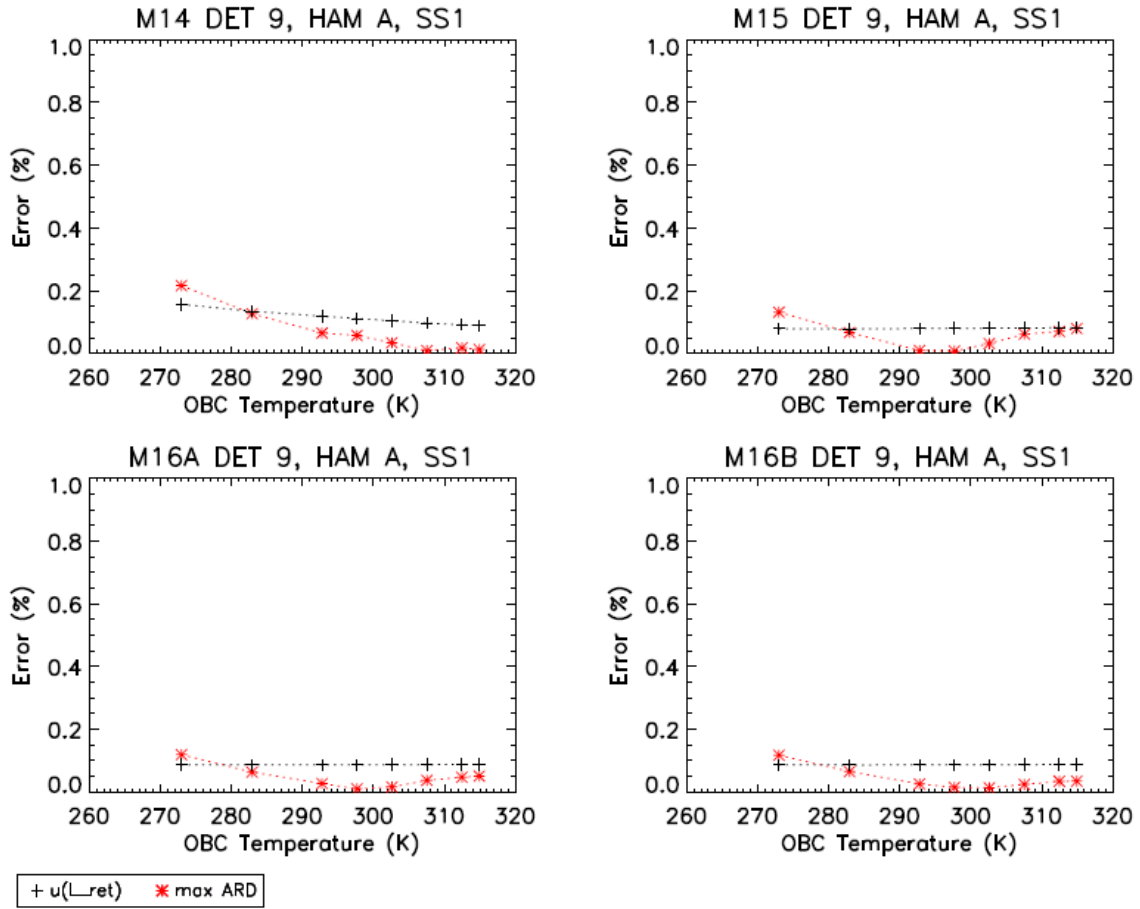


Figure 27: Total uncertainties in OBC L_{ret} across instrument conditions.

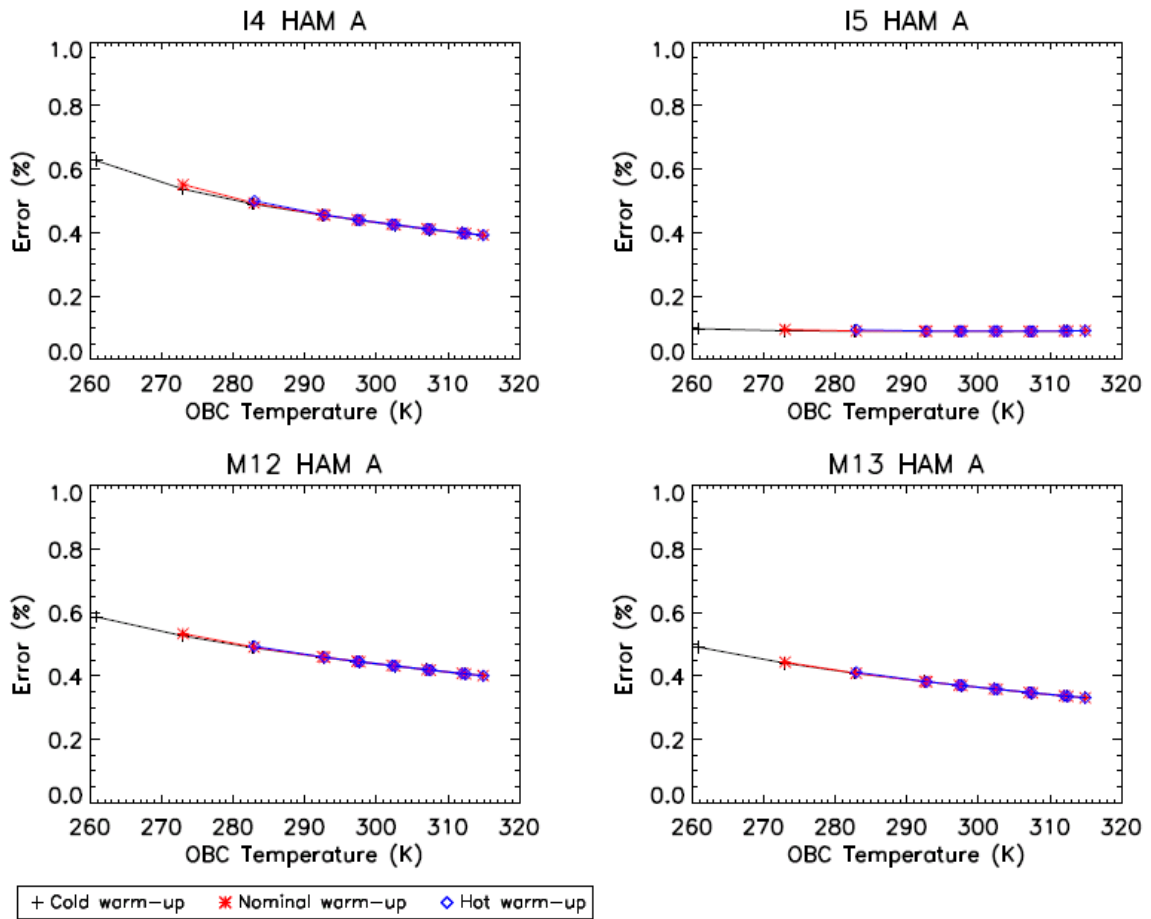


Figure 28: Total uncertainties in OBC L_{ret} across instrument conditions.

